Available online at www.sciencedirect.com
SCIENCE DIRECT®
Journal of Nuclear Materials 329–333 (2004) 278–282
journal of nuclear materials
www.elsevier.com/locate/jnucmat

Tensile properties of a tempered martensitic iron–chromium–carbon model alloy

R. Bonadé [a,*], P. Spätig [a], M. Victoria [a], T. Yamamoto [b], G.R. Odette [b]

[a] *Fusion Technology Materials, CRPP-EPFL, Association EURATOM-Confederation Suisse, ODGA-109, 5232 Villigen PSI, Switzerland*

[b] *Department of Mechanical and Environmental Engineering, University of California Santa Barbara, 3343 Engineering II, Santa Barbara, CA 93106, USA*

Abstract

A detailed study of the strain-hardening on a Fe–9Cr–0.1C tempered martensitic model alloy has been undertaken in the temperature range of 77–343 K. The true stress–true strain curves were calculated from tensile test data. In the framework of a phenomenological model for the strain-hardening based on dislocation mechanics, it has been shown that, above 170 K, the whole post-yield behavior can be reasonably described by a single law. On the contrary, below 170 K, a careful examination of the strain-hardening indicated that the single law cannot describe anymore the entire post-yield strain range. It has been suggested that this behavior is related to the low mobility of the screw dislocations in the low temperature regime that influences the shape of the tensile curve.

1. Introduction

The tempered martensitic steels are among the most promising candidate materials for structural applications in fusion reactor [1]. A great deal of studies on these steels have been undertaken, in the framework of the international fusion material development program, to investigate and characterize the mechanical and physical properties in relation to their microstructures [2] and their evolution and stability under irradiation [3]. As far as the tensile properties are concerned, the main effort has been focused on the irradiation-induced hardening and the loss of ductility, [4–6]. However, some investigations have been done to characterize the overall shape of the tensile curves and the temperature dependence of the strain-hardening [7,8], the effect of precipitates on the work-hardening [9] and to model the flow localization and ductiliy loss [10]. The strain-hardening law that we presented in [8] was based on a simplified model of dislocations mechanics for the F82H tempered martensitic steels. The model was successfully applied in the temperature range 200–723 K. The goal of this paper is to present new tensile data obtained on a Fe–9Cr–0.1C tempered martensitic model alloy for temperature ranging from 77 K up to 343 K and to analyze the evolution of the strain-hardening law.

2. Experimental procedure

A Fe–Cr–C model alloy with 9 wt% Cr and 0.1 wt% C, produced by Carpenter Technology Corporation, has been studied in this work. The heat-treatment of this steel consisted of an austenization at 1253 K during 25 min and air quenching followed by a tempering at 863 K during 80 min. The microstructure of the alloy has been fully characterized by optical and transmission electron microscopy. Basically, it presents a fully tempered martensitic microstructure. The mean intercept length of the prior austenitic grains was about 27 μm. Details about the microstructural characterization can be found in [11].

* Corresponding author. Tel.: +41-56 310 29 41; fax: +41-56 310 45 29.
E-mail address: raul.bonade@psi.ch (R. Bonadé).

0022-3115/$ - see front matter © 2004 Elsevier B.V. All rights reserved.
doi:10.1016/j.jnucmat.2004.04.054

Tensile tests were carried out with a Schenck RMC100 electro-mechanical testing machine. Standard DIN round specimens were used with 3 mm diameter and 18 mm gauge length. The tests were performed at several temperatures from 77 K up to 343 K. A temperature chamber was mounted around the load train. Temperature control was provided by a PID controller along with a regulated N_2 gas flow. In all the cases, the temperature variation on the specimen during testing was less than 0.5 K. The tests were performed at a constant crosshead velocity of 0.1 mm/min corresponding to a nominal strain-rate of 9.3×10^{-5} s^{-1}. At all temperatures but room temperature, the elongation of the specimens was deduced from the displacement of the machine crosshead measured with a linear variable differential transformer (LVDT) by using a compliance correction. The consistency of the compliance correction procedure was checked at room temperature by comparing the corrected data obtained from the LVDT extensometer with that obtained from a clip gauge attached to the gauge length of a specimen. The stresses and strains reported hereafter are the true stress and true strain.

In order to investigate the strain-hardening behavior, the flow stress was decomposed into two components, namely, the yield stress $\sigma_{0.2}$, defined at 0.002 plastic strain, and the so-called plastic stress σ_{pl} defined as $\sigma_{pl} = \sigma - \sigma_{0.2}$. In the following plots of σ_{pl} versus ε_{pl}, the origin of the plastic strain axis was chosen at the yield stress so that ε_{pl} is defined as

$$\varepsilon_{pl} = \varepsilon - \frac{\sigma(\varepsilon)}{E(T)} - 0.002, \tag{1}$$

where $\sigma(\varepsilon)$ is the true flow stress, ε is the total true strain and $E(T)$ is the Young modulus, slightly dependent on temperature. The temperature dependence of E was assimilated to that of the F82H steel and calculated from [12]. Finally, the strain-hardening θ is defined as

$$\theta = \frac{d\sigma_{pl}}{d\varepsilon_{pl}}. \tag{2}$$

3. Results and discussion

The temperature dependence of yield stress, $\sigma_{0.2}$, is presented in Fig. 1. As expected for this type of alloy and consistently with other data on tempered martensitic steels [13], a strong increase of the yield stress with decreasing temperature is observed below 200 K. This temperature dependence is attributed to an intrinsic Peierls type mechanism acting on the screw dislocations while much weaker thermally activated processes take place between 200 and 300 K. $\sigma_{0.2}$ at 350 K indicates that the plastic flow becomes completely athermal above

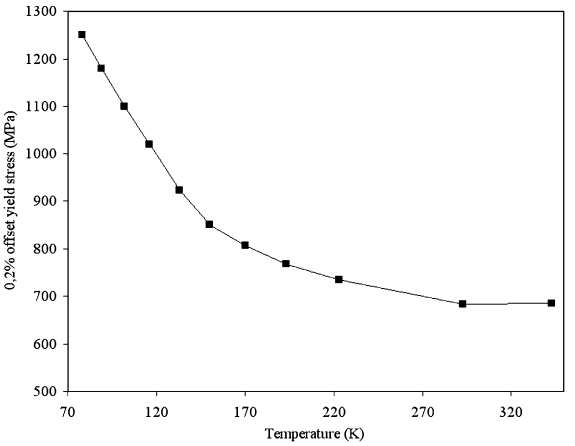

Fig. 1. Temperature dependence of the yield stress.

room temperature. Being interested in possible consequences of the absolute value of $\sigma_{0.2}$ and of temperature as well on the subsequent post-yield behavior, we focus in the following on the strain-hardening behavior. The post-yield stress–strain data are presented in Fig. 2 for a broad range of temperatures. For the sake of clarity, only the data below 170 K are included in Fig. 2(a). In Fig. 2(b), we present two $\sigma_{pl}(\varepsilon_{pl})$ curves, one at 150 K belonging to the highly thermally activated regime of the yield stress and one at 293 K corresponding to the athermal one. The curves in Fig. 2(a) exhibit an interesting behavior; for a certain ε_{pl} the corresponding σ_{pl} increases with temperature. This behavior does not hold for temperatures higher than 170 K where the $\sigma_{pl}(\varepsilon_{pl})$ curve shows a much more pronounced curvature resulting in a more rapid decrease of the strain-hardening rate with strain as can be seen in Fig. 2(b) at 293 K.

The strain-hardening, deduced from the experimental $\sigma_{pl} - \varepsilon_{pl}$ curves, is presented in Fig. 3(a) and (b) respectively as a function of σ_{pl}. Although the tensile test does not allow us to explore the plastic behavior up to large strains due to the necking instability, it was still possible to observe a change in the strain-hardening behavior with temperature. Indeed, independently from the temperature considered, an initial region is observed where the strain-hardening strongly decreases with σ_{pl}. In the case of temperatures above 170 K, a second region characterized by an almost linear decrease of the strain-hardening with σ_{pl} is observed at higher σ_{pl}. These two regions are illustrated in Fig. 3(b) where the strain-hardening at 293 K is presented as an example of the high temperature behavior. In the case of temperatures below 170 K an intermediate region of the strain-hardening develops between the two regions described previously. This intermediate region is clearly promoted by decreasing temperature as is shown in Fig. 3(a). The case of the 77 K curve is certainly interesting since the

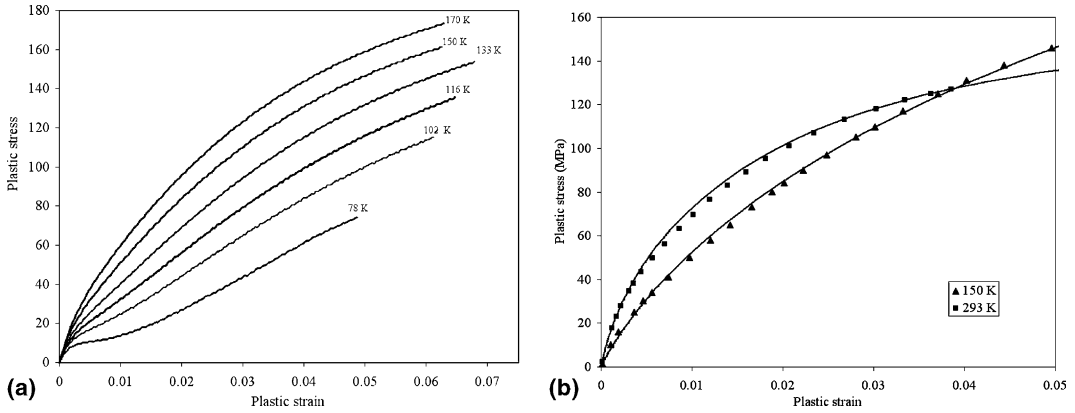

Fig. 2. (a) Plastic stress–plastic strain curves at low temperatures, (b) plastic stress–plastic strain curve at 293 K with fit according to Eq. (5). At 293 K, $P_1 = 580000$ MPa^2, $P_2 = 18$, $\sigma_0 = 29$ MPa. A low temperature example (150 K) is also included. In this last case, the parameters values are $P_1 = 462750$ MPa^2, $P_2 = 3.5$, $\sigma_0 = 57$ MPa.

strain-hardening exhibits a minimum after the initial parabolic region. Furthermore, at 77 K it has to be mentioned that the load has been observed to slightly decrease after the yield point by about 36 N from the absolute 8800 N reached of the yield point. Finally, for plastic stress values larger than 60 MPa, the strain-hardening displays the same linear decrease with σ_{pl} than the higher temperature examples.

This continuous decrease of θ with σ_{pl} suggests that a saturation stress, σ_{sat}, would be reached at which the strain-hardening becomes zero. In fact, σ_{sat} can be readily estimated by extrapolation of the $\theta(\sigma_{pl})$ curves at high stresses, where the decrease is practically linear. Nonetheless, this hypothesis cannot be fully supported by the tensile tests data presented here since higher strain levels should be analyzed in order to discard the potential existence of a strain-hardening stage IV (or even V) at large strains, as observed in other metals [14], that may significantly modify the value of σ_{sat}.

Following the phenomenological description of the strain-hardening initially developed by Kocks and Mecking [15,16] and later by Mecking and Estrin [17], we already showed that the strain-hardening in tempered martensitic steels can be represented by the following equation [11]:

$$\theta = \frac{P_1}{(\sigma_{pl} + \sigma_0)} - P_2(\sigma_{pl} + \sigma_0). \tag{3}$$

Let us remind that this equation is derived by assuming that the flow stress increase is due to the net storage of dislocations in the material and that $(\sigma_{pl} + \sigma_0)$ follows the Taylor's equation [18]:

$$\sigma_{pl}(\varepsilon_{pl}) + \sigma_0 = M\alpha\mu b\sqrt{\rho} = M\alpha\mu b\sqrt{\rho_0 + \Delta\rho(\varepsilon_{pl})}, \tag{4}$$

where M is the Taylor factor, α is a dimensionless constant, μ is the shear modulus, b is the magnitude of the

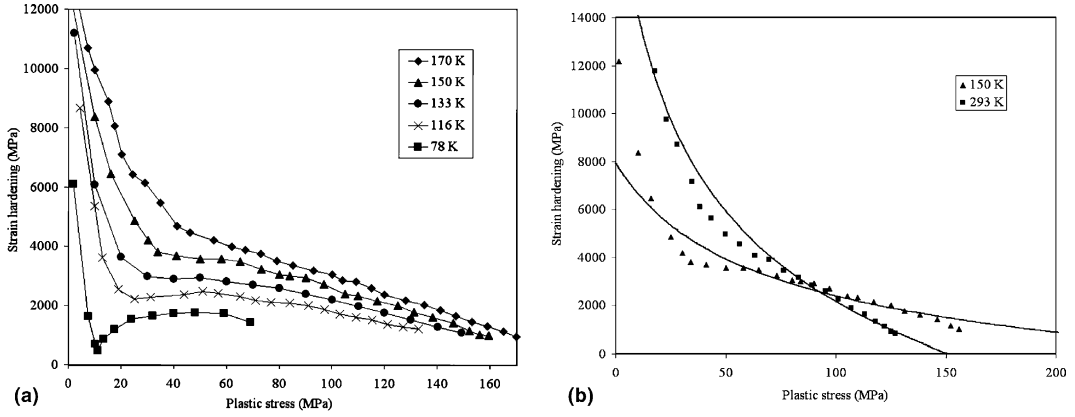

Fig. 3. (a) Strain-hardening versus σ_{pl} at low temperatures, (b) strain-hardening versus σ_{pl} at high temperatures with fit according to Eq. (3).

Burgers vector and ρ_0 is the grown-in dislocation density. Note that in Eq. (3) σ_0 is equal to $M\alpha\mu b\sqrt{\rho_0}$ and that P_1 and P_2 are coefficient reflecting the storage and annihilation of the dislocations via an effective mean displacement distance and annihilation distance that are assumed constant with deformation. The Eq. (3) can be integrated to obtain $\sigma_{pl} = \sigma(\varepsilon_{pl})$, yielding

$$\sigma_{pl} = \sqrt{\frac{P_1 - (P_1 - P_2\sigma_0^2)\exp(-2P_2(\varepsilon_{pl}))}{P_2}} - \sigma_0. \quad (5)$$

Thus, the $\sigma_{pl}(\varepsilon_{pl})$ experimental data can be fitted using the above equation by adjusting P_1, P_2 and σ_0 parameters. It is worth noting that Eq. (5) leads to a saturation stress σ_{sat} equal to $(P_1/P_2)^{0.5} - \sigma_0$. Two examples of fits are given in Fig. 2(b) at 293 and 150 K where it can be seen that the fits are qualitatively good. However, keeping in mind that three-parameter fits are used to reconstruct the deformation curves over a limited strain range, special attention has to be paid to the self-consistency of the analysis. In particular, it was found that the fitted parameter σ_0 was temperature-dependent. Indeed, at room temperature $\sigma_0 = 29$ MPa while at 150 K $\sigma_0 = 57$ MPa. However, according to its definition, σ_0 depends only on the initial dislocation density and a variation from 29 MPa to 57 MPa would correspond to an increase of ρ_0 by a factor of about 3.8, which is obviously not consistent. Clearly, the good quality of the fits does not warrant the physical meaning of the fitting parameters. If the model is self-consistent, the strain-hardening can be recalculated by using the fitted parameters obtained from Eq. (5) and compared with the experimental data. This comparison is shown in Fig. 3(b) for two temperatures, namely 293 and 150 K. It can be seen that, at 293 K, the calculated $\theta(\sigma_{pl})$ curve predicts satisfactorily well the data, when the fitting parameters extracted from Eq. (5) are used. Note however that between about 40 and 60 MPa the calculated strain-hardening is slightly higher than the data. A close look at Fig. 2(b) reveals that the fit slightly overestimates the experimental stress–strain curve by only few MPa between $\sigma_{pl} = 40$ and 70 MPa. It is worth mentioning that an extrapolation of the data at 293 K (Fig. 3(b)) to zero gives a saturation stress equals to 150 MPa ± 10 MPa while the calculated saturation stress from the fitting parameters ($\sigma_{sat} = (P_1/P_2)^{0.5} - \sigma_0$) is 150 MPa. In this case, the strain-hardening law and its integrated law predicts well the $\sigma_{pl}(\varepsilon_{pl})$ and $\theta(\sigma_{pl})$ experimental curves as well as the saturation stress. On the contrary, at $T = 150$ K, the good fitting of the $\sigma_{pl}(\varepsilon_{pl})$does not translate into a good prediction of the strain-hardening versus σ_{pl} as it can be seen in Fig. 3(b). First, at this last temperature, the calculated θ_p is much lower than the measured one in the initial stage of plastic deformation and does not reproduce properly the linear decrease at high stress. The direct consequence of this observation is that an estimation of the saturation stress from the fitting parameters would yield an erroneous value. In this specific case, we obtain $\sigma_{sat} = 300$ MPa while a direct extrapolation of the data to high stress give about 190 MPa.

The above observations allow us to identify two temperature domains for the strain-hardening behavior. The first one corresponds to temperature below 170 K and the second one above this last temperature. In the high temperature domain, Eq. (3) provides a good description of the strain-hardening law, at least over the whole tensile curve. In other words, plastic flow can be satisfactorily described by a simple model of dislocation mechanics with one single structural parameter, the total dislocation density ρ and two characteristic distances, the mean displacement distance of dislocations and an annihilation distance, which are taken into account via the coefficients P_1 and P_2. Eq. (3) does not hold any more below 170 K. As described above, the $\theta(\sigma_{pl})$ curves shown in Fig. 3(a) indicate that the three identified regions of strain-hardening cannot be described by Eq. (3) characterizing a monotonous decrease. It is worth noting that the temperatures lower than 170 K correspond to those at which the Peierls mechanism controls the dislocation mobility. In this low temperature regime, the non-screw segments of the dislocation loops moves first at low strains increasing the screw dislocation density only. This approach was used to model the evolution of the dislocation density at low strain in bcc metals by Essmann and Mughrabi [19]. After a certain amount of strain, dependent on temperature, the motion of the screw segments can no longer be disregarded that leads to an additional increase of the non-screw segments. The intermediate region of strain-hardening that we observed could be explained on that basis.

4. Summary

Tensile tests were carried out on a Fe–9Cr–0.1C model alloy for temperatures ranging from 77 K up to 343 K at constant nominal strain rate of 9.3×10^{-5} s^{-1}. The strain-hardening was analyzed as a function of the stress. It was found that the strain-hardening can be reasonably described in the framework of the phenomenological approach of Kocks and Mecking for temperature above 170 K. A single strain-hardening law was found to describe reasonably the whole tensile curve. In this model, only three key parameters are used, namely the total dislocation density, the mean displacement distance of the mobile dislocations and the effective annihilation distance. By decreasing temperature, it was found that the single law does not hold anymore and a more sophisticated description of the strain-hardening needs to be elaborated. It was suggested that the limited mobility of the screw dislocations resulting in an

increase of the screw dislocation density first followed by an increase of the non-screw dislocation density at higher strains may be the basis for further developments.

Acknowledgements

The financial support of EURATOM and of the Swiss National Foundation are gratefully acknowledged. The Paul Scherrer Institute is acknowledged for the overall use of facilities.

References

[1] R. Klueh, D.S. Gelles, S. Jitsukawa, A. Kimura, G.R. Odette, B. van der Schaaf, M. Victoria, J. Nucl. Mater. 307–311 (2002) 455.
[2] M. Victoria, D. Gavillet, P. Spätig, F. Rezai-Aria, S. Rossmann, J. Nucl. Mater. 233–237 (1996) 326.
[3] D.S. Gelles, J. Nucl. Mater. 212–215 (1994) 714.
[4] R.L. Klueh, J.M. Vitek, J. Nucl. Mater. 161 (1989) 13.
[5] F. Abe, M. Narui, H. Kayano, Mater. Trans. JIM 34 (11) (1993) 1053.
[6] N. Baluc, R. Schäublin, C. Bailat, F. Paschoud, M. Victoria, J. Nucl. Mater. 283–287 (2000) 731.
[7] P. Spätig, N. Baluc, M. Victoria, Mater. Sci. Eng. A 309–310 (2001) 425.
[8] P. Spätig, G.R. Odette, E. Donahue, G.E. Lucas, J. Nucl. Mater. 283–287 (2000) 721.
[9] D. Preininger, J. Nucl. Mater. 307–311 (2002) 514.
[10] G.R. Odette, M.Y. He, E.G. Donahue, P. Spätig, T. Yamamoto, J. Nucl. Mater. 307–311 (2002) 171.
[11] R. Bonadé, P. Spätig, R. Schäublin M. Victoria, Mater. Sci. Eng., submitted for publication (2004).
[12] K. Edsinger, PhD thesis, University of California, Santa Barbara, 1995, p. 115.
[13] P. Spätig, G.R. Odette, G.E. Lucas, J. Nucl. Mater. 275 (1999) 324.
[14] M. Zehetbauer, V. Seumer, Acta Met. Mater. 41 (1993) 557.
[15] U.F. Kocks, J. Eng. Mater. Tech. ASME H 98 (1976) 76.
[16] H. Mecking, U.F. Kocks, Acta Met. 29 (1981) 1865.
[17] Y. Estrin, H. Mecking, Acta Met. 32 (1984) 57.
[18] G.E. Dieter, Mechanical Metallurgy, McGraw-Hill, London, 1988, p. 232.
[19] U. Essmann, H. Mughrabi, Philos. Mag. A 40 (1979) 731.